DOI: 10.1002/adsc.201300447

Ruthenium-Catalyzed Transvinylation – New Insights

Jennifer Ziriakus,[+a,b] Teresa K. Zimmermann.,[+a] Alexander Pöthig,[a] Markus Drees,[a] Stefan Haslinger,[a] Dominik Jantke,[a] and Fritz E. Kühn[a,*]

[a] Chair of Inorganic Chemistry/Molecular Catalysis, Catalysis Research Center, Technische Universität München, Ernst-Otto-Fischer Straße 1, 85747 Garching b. München, Germany
Fax: (+49)-89-289-13473; e-mail: fritz.kuehn@ch.tum.de

[b] WACKER-Institut für Siliciumchemie, Department of Chemistry, Technische Universität München, Ernst-Otto-Fischer Straße 1, 85747 Garching b. München, Germany

[+] J. Z. and T. K. Z. contributed equally to this work.

Received: May 22, 2013; Revised: September 4, 2013; Published online: October 9, 2013

Supporting information for this article is available on the WWW under http://dx.doi.org/10.1002/adsc.201300447.

Abstract: The use of ruthenium complexes in transvinylation catalysis has been well established since the 1980s. However, the reaction mechanism and the active catalyst species, which is presumed to contain ruthenium carbonyl carboxylate entities, have so far remained elusive. In this work the synthesis and characterization of three novel ruthenium complexes comprising ruthenium carbonyl carboxylate structural motifs including two single crystal structures as well as the crystal structures of two known ruthenium complexes are reported. These new complexes and four known ruthenium complexes with appropriate structural motifs were applied in transvinylation catalysis. Mechanistic studies including identification and characterization of the active species, isotope labeling experiments and examination of the regio- and stereoselectivity of the transvinylation reaction are presented, resulting in the proposal of a probable reaction mechanism, which is supported by DFT calculations on the B3LYP/6-31G* level of theory.

Keywords: carbonyl ligands; carboxylate ligands; reaction mechanisms; reactive intermediates; ruthenium

Introduction

Vinyl esters are frequently used in industrial applications such as paint production,[1] medical products,[2] paper coatings,[3] and construction materials,[4] as well as in organic synthesis and pharmaceutical chemistry.[5] Thus, a wide variety of methods has been developed for their preparation. These include oxidative acetoxylation of olefins using $Pd(OAc)_2$[6] and direct addition of carboxylic acids to terminal alkynes catalyzed by mercury salts,[7] Ru,[8] Rh[9] or Ir[10] complexes. The synthetic approach *via* transvinylation of carboxylic acids with vinyl donors has been reported using Hg(II)[11] and Pd(II)[12] materials as well as a series of ruthenium precursors such as ruthenium carbonyls, ruthenocene or ruthenium trichloride hydrate.[13] The advantages of ruthenium-catalyzed transvinylation include the accessibility of functionalized vinyl ester building blocks, lower toxicity compared to mercury-based reactions, accessibility of thermally labile vinyl esters and increased stability compared to Pd(II) systems. Despite a number of patents claiming the use of different ruthenium precursor species for ruthenium-catalyzed transvinylation,[13a–c] to the best of our knowledge mechanistic details have never been studied. We present here a mechanistic study of the catalytic pathway including isotope-labeling experiments and examination of regio- and stereoselective aspects. Based on the experimental results, we propose a plausible reaction mechanism. Three novel and four known ruthenium complexes were synthesized and characterized in order to emulate relevant catalyst structural motifs. The reaction mechanism is supported by DFT calculations on the B3LYP/6-31G* level of theory.

Results and Discussion

Structural Motif of the Active Catalyst Species

Patent literature states that a variety of ruthenium compounds can be used to generate the catalyst for transvinylation *in situ*. The empirical formula

$[Ru(CO)_2(RCO_2)]$ is assigned to this catalyst,[13c] therefore the most active ruthenium precursors are believed to be ruthenium carbonyl compounds.[13d] However, $RuCl_3$ hydrate may also be used as precursor for efficient transvinylation catalysis, which is preferential due to the significantly lower cost.[13a] In a typical reaction 0.5–5 mol% of the ruthenium precursor, and an up to ten-fold excess of vinyl donor relative to the amount of carboxylic acid are used. If $RuCl_3$ hydrate is used as ruthenium source, the addition of an alkali salt such as sodium acetate or sodium hydroxide is necessary for satisfactory transvinylation activity.[13] Transvinylations are equilibrium reactions which typically exhibit equilibrium constants close to 1 (Scheme 1).[13d]

Based on these observations, a model catalytically active mixture using 2 mol% $RuCl_3$ hydrate, 2 mol% NaOH, vinyl acetate and propionic or valeric acid as model substrates in a molar ratio of 2.7:1 (vinyl acetate:carboxylic acid) was prepared and analyzed.

All volatiles were removed under vacuum after completion of the reaction. IR spectroscopy was used to analyze the obtained solid residue. Three strong carbonyl absorption bands were observed. The two bands at 2131 cm^{-1} and 2059 cm^{-1} indicate the presence of three CO ligands within a mononuclear Ru(II) species. The relatively high frequency carbonyl absorption bands are in a typical range for *fac*-ruthenium(II) tricarbonyls.[14] ^{13}C NMR spectroscopy shows a carbonyl signal at 196.2 ppm, further substantiating the presence of carbonyl ligands. Electrospray mass spectrometry of the crude reaction mixture reveals the presence of a dinuclear $[Ru_2(CO)_4(RCOO)_2(L^1)(L^2)]^-$ species as well as a mononuclear $[Ru(CO)_3(R^1COO)(R^2COO)]^-$ species (Figure 1). Fragmentation patterns clearly indicate the presence of three carbonyl ligands in both cases.

From these results, taking into account the unequal intensity of the CO vibrational frequencies in the IR and the presence of dinuclear species as evidenced *via* ESI-MS, a mixture of the two species displayed in Figure 1 is proposed to be present in the reaction mixture formed from alkaline $RuCl_3$ hydrate.

The carbonyl pattern in the IR spectrum is in accordance with the two proposed active species and was confirmed by DFT calculations (B3LYP/6-31G*) (Figure 2). Assuming a mixture of both species, the IR spectrum exhibits the band structure and absorption intensities as expected. Differences in the lower

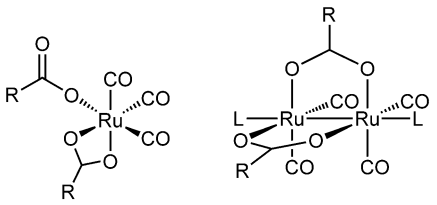

Figure 1. Proposed structure of the Ru(II) (*left*) and Ru(I) (*right*) species in the active reaction mixture. L = H_2O, Cl^- or CH_3COOH; R = CH_2CH_3, CH_3.

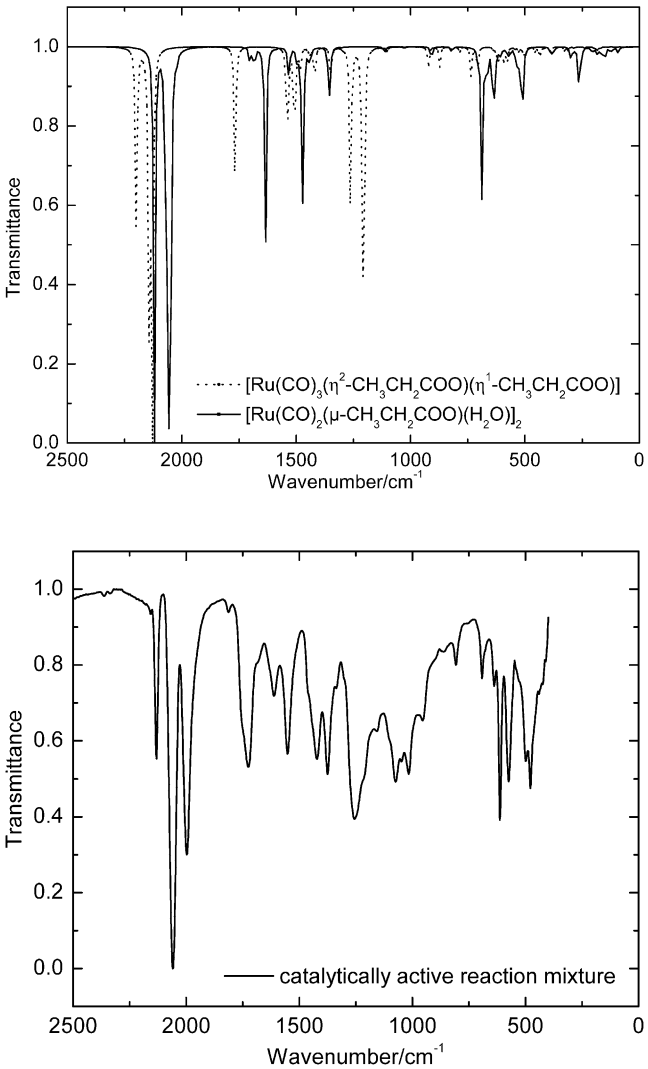

Figure 2. Calculated IR spectra for the model compounds (*top*) and experimental spectrum of the dried reaction mixture (*bottom*).

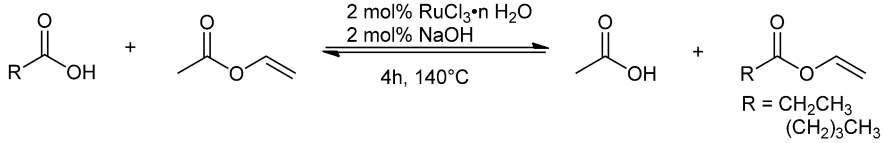

Scheme 1. Reaction scheme for the model transvinylation reaction with propionic acid and valeric acid as model substrates.

frequency region result from organic residuals in the catalytically active crude mixture.

From the catalytically active crude mixture, different ruthenium carbonyl carboxylate species could be isolated and characterized. The mononuclear salt Na-[*fac*-Ru(CO)$_3$(CH$_3$COO)$_3$] (**1**) was obtained after evaporation of all volatiles, washing with diethyl ether and recrystallization from THF (see Figure 3). Crystallographic data are given in Table 1. The anionic complex crystallizes in the non-centrosymmetric space group P-1 and exhibits a *fac* configurated octahedral coordination sphere. Within the limits of the experimental error, equivalent bond lengths are equal. The octahedral structure is slightly distorted, resulting in *trans*-bonding angles of 171.42(14) to 175.55(16) deg. The *fac* carboxylate ligands are allocated in close proximity due to mutual coordination by both sodium and ruthenium, while the carbonyl ligands spread out. This is reflected in the *cis*-bonding angles of 79.78(9), 80.68(10), 82.52(9) deg between the carboxylate ligands, while the respective angles between carbonyl ligands range from 89.16(18) to 91.61(17) deg. The bonding angles intermittent between one carboxylate and one carbonyl ligand are found in the range of 92.09(14) to 96.42(15) deg.

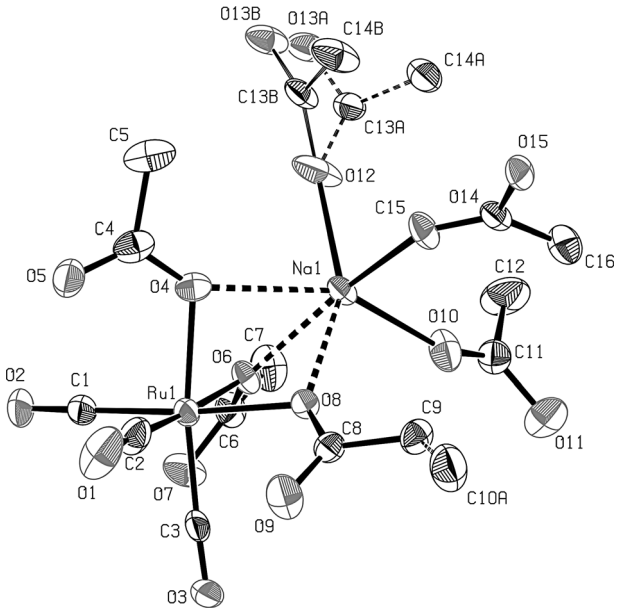

Figure 3. ORTEP representation of Na[*fac*-Ru(CO)$_3$(CH$_3$COO)$_3$] (**1**) as isolated from the crude reaction mixture. Thermal ellipsoids are shown at the 30% probability level. Protons are omitted for clarity. Selected bond lengths (Å) and bond angles (deg): Ru1–C1 1.910(4), Ru1–C2 1.909(4), Ru1–C3 1.905(4), Ru1–O4 2.079(3), Ru1–O6 2.082(2), Ru1–O8 2.085(2), Na1–O10 2.327(4), Na1–O12 2.297(4), Na1–O14 2.326(3), O4–Ru1–C3 171.52(14), O6–Ru1–C2 175.55(16), O8–Ru1–C1 173.21(14), O4–Ru1–O6 79.78(9), O4–Ru1–O8 80.68(10), O6–Ru1–O8 81.52(9), O6–Ru1–C1 92.49(14), O4–Ru1–C1 95.16(14), O4–Ru1–C2 96.01(15), O8–Ru1–C2 96.42(15), O8–Ru1–C3 92.09(14), C1–Ru1–C2 89.33(19), C1–Ru1–C3 91.61(17), C2–Ru1–C3 89.16(18).

Table 1. Crystallographic data for complexes **1** and **3**.

	1	**3**
Formula	$C_{15}H_{22}NaO_{15}Ru$ (81%) $C_{16}H_{24}NaO_{15}Ru$ (19%)	$C_{14}H_{22}O_{10}Ru_2S_2$
Formula wt	568.13	616.60
Space group	*P-1*	*P* $2_1/c$
a (Å)	11.1566(9)	15.941(2)
b (Å)	12.327(1)	8.5929(11)
c (Å)	12.4777(10)	16.887(2)
α (deg)	66.021(3)	90
β (deg)	63.565(3)	100.662(3)
γ (deg)	77.624(3)	90
V (Å^3)	1402.8(2)	2273.2(5)
Z	2	4
$D_{calcd.}$ (g cm^{-3})	1.345	1.802
N_{ref}	5091	4009
N_{par}	351	259
R1 ($I > 2\sigma(I)$)	0.0386	0.0210
wR2 (all data)	0.1028	0.0548
Goodness of fit	1.144	1.04

In 19% of the crystallized species, one of the acetate ligands is exchanged for a propionate ligand. This substitution is always observed at the same carboxylate ligand position, i.e., overall an exchange of about $0.19 \times 0.33 = 0.06$ (6%) of acetate ligands in favor of propionate ligands can be observed in the crystal. This mixture of carboxylate ligands can be attributed to the presence of both acetic acid and propionic acid in the reaction mixture in a ratio of 1:1 after about 3 h. It is evident from the integrals in the ^{1}H NMR spectrum that the carboxylate ligand positions are occupied in a 1:1 ratio by propionate and acetate in solution. The observed signal positions appear shifted slightly upfield compared to the isolated carboxylic acids, which is attributed to π-backbonding of the ruthenium metal center. The carbonyl signal in the ^{13}C NMR spectrum is observed at 196.2 ppm. The observation of only two carbonyl absorption bands in the IR spectrum of the crystallized species at 2127 cm^{-1} and 2049 cm^{-1} provides evidence for the predominant symmetrical occupation of the carboxylate ligand positions with three acetates. The relatively high frequency absorption band at 2127 cm^{-1} is in a typical range for *fac*-ruthenium(II) tricarbonyls.[14] The large difference of 239 cm^{-1} between ν_{sym} and ν_{asymm} of the carboxylate vibration band illustrates the monodentate binding mode of the carboxylate ligands.[15]

In contrast to the previously reported salt [(*n*-Pr)$_4$N][*fac*-Ru(CO)$_3$(CH$_3$COO)$_3$],[16] the Na$^+$ cation within the crystal structure interacts directly with three ruthenium-coordinated carboxylate ligands and

accounts for the co-crystallization of three additional acetates. Na^+ itself is thus coordinated by six carboxylate ligands overall in a distorted octahedral manner.

After addition of water to the reaction mixture, carboxylate-bridged ruthenium polymers of the type $[Ru(CO)_2(RCOO)]_n$ [$R = CH_2CH_3$,[17] $(CH_2)_5CH_3$ depending on the substrates used] can be isolated and identified *via* ^1H and ^{13}C NMR spectroscopy (Figure 4). The valerate bridged polymer has not

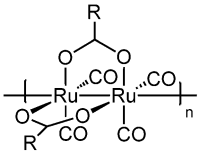

Figure 4. $[Ru(CO)_2(RCOO)]_n$ as isolated from the reaction mixture. $R = CH_2CH_3$, $(CH_2)_3CH_3$ (**2**).

been reported so far. For synthetic purposes, it may also be synthesized according to the general procedure for $[Ru(CO)_2(RCOO)]_n$-type polymers published by Lewis et al. in 1969.[17] Upon addition of DMSO, a new dimeric species $[Ru(CO)_2(\mu\text{-}CH_3CH_2COO)(dmso)]_2$ (**3**) is formed and can be isolated as yellow crystals. This complex is a new representative of dimeric ruthenium complexes of the type $[Ru(CO)_2(RCOO)_2(L)]_2$, which have been known since the 1960s.[17,18] The crystal structure is shown in Figure 5, crystallographic data are given in Table 1.

The complex crystallizes in a monoclinic system in the space group $P2_1/c$ and exhibits a typical sawhorse structure, with two bridging propionate ligands in the paddlewheel positions. In *trans*-position to every carboxyl-O atom is a carbonyl ligand. The geometry is slightly bent, which is reflected in *trans*-bonding angles of 175.39(10) deg to 177.68(10) deg. The axial DMSO ligands are distorted towards the propionate ligands, which results in bonding angles along the respective Ru1–Ru2–S axes below 170 deg. Interestingly, the methyl groups are oriented towards the propionate ligands, possibly due to interaction of propionate-O with methyl-H atoms. The DMSO-oxygen atoms are directed towards the carbonyl ligands. Within the limits of the experimental error, equivalent bond lengths are equal.

In the ^1H NMR spectrum, the DMSO signal appears with a significant downfield shift of 0.38 ppm at 3.00 ppm in $CDCl_3$ compared to the free solvent molecule, illustrating the reduced electron density due to ruthenium coordination. The propionate signals appear shifted slightly upfield compared to free propionic acid, indicating π-backbonding of the ruthenium metal center to the carboxylate ligands.

Even though complexes with structures similar to those that were isolated from the crude transvinylation reaction mixture are well known in the literature

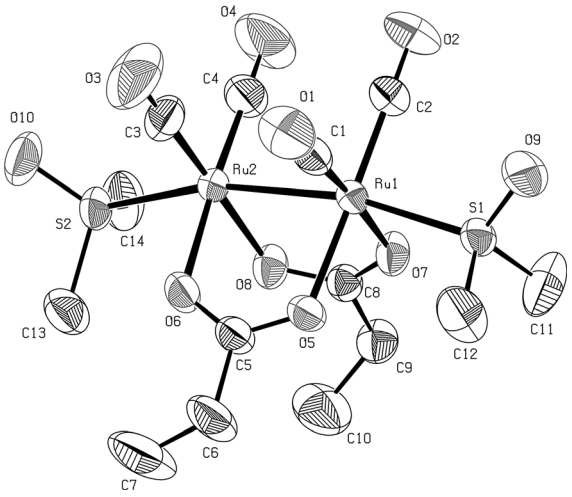

Figure 5. ORTEP representation of $[Ru(CO)_2(\mu\text{-}CH_3CH_2COO)(dmso)]_2$ (**3**) as isolated from the reaction mixture upon addition of DMSO. Thermal ellipsoids are shown at the 50% probability level. Protons are omitted for clarity. Selected bond lengths (Å) and bond angles (deg): Ru1–Ru2 2.6678(4), Ru1–S1 2.4081(7), Ru2–S2 2.4214(8), Ru1–O5 2.1191(18), Ru2–O6 2.1166(18), Ru1–O7 2.1203(17), Ru2–O8 2.1088(18), Ru1–C1 1.846(3), Ru2–C3 1.838(3), Ru2–Ru1–S1 167.40(2), Ru1–Ru2–S2 165.71(2), O5–Ru1–O7 84.05(7), O6–Ru2–O8 83.13(7), O5–Ru1–C1 91.40(10), O6–Ru2–C3 94.23(12), O7–Ru1–C2 94.63(9), O8–Ru2–C4 93.41(12), C1–Ru1–C2 89.89(12), C3–Ru2–C4 89.20(15), O5–Ru1–C2 177.68(10), O6–Ru2–C4 176.23(12), O7–Ru1–C1 175.39(10), O8–Ru2–C3 176.97(12).

(see above), neither $[Ru(CO)_3(RCOO)_3]^-$ nor $[Ru(CO)_2(RCOO)(L)]_2$-type complexes have been employed in transvinylation catalysis so far.

In a more general manner, Ru-carbonyl-carboxylate species have been suggested before by Murray as active catalysts in transvinylation reactions.[13a–c] In his patents from the late 1980s/early 1990s, he identifies "$[Ru(CO)_2RCO_2]$" as the active species.[13c] It is stated that the choice of ruthenium precursor is not critical for the reaction to proceed. This indicates that the same active species is formed regardless of the provided ruthenium source if the reaction conditions are chosen in an appropriate manner.

Catalytic Activity

The following comparison of the catalytic activity of defined ruthenium carbonyl carboxylates in transvinylation catalysis aims at confirming the structural motifs of the active catalyst species as proposed in the previous section (Figure 1). In addition, the reactivity of mononuclear and dinuclear ruthenium complexes is compared in order to elucidate the role of the two proposed structures of the active species.

Synthesis of Reference Compounds

Figure 6 provides an overview over the ruthenium catalysts applied. Complexes **5**,[14] **6**,[19] **7**[20] and **8**[17] were synthesized according to known literature procedures; **1**, **3**, and **4** are new complexes, which have not been reported so far. For synthetic purposes, complex **3** is formed from the $[Ru(CO)_2(CH_3CH_2COO)]_n$ polymer **8**, which is recrystallized from DMSO to form

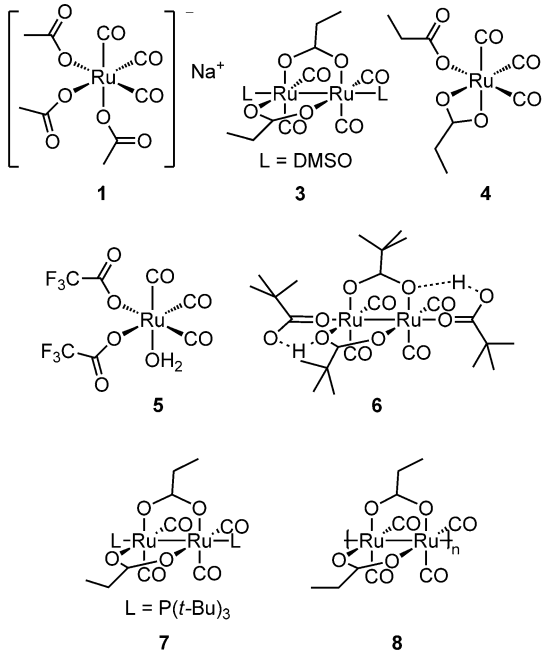

Figure 6. Catalyst complexes used for comparison with the catalytically active crude mixture.

the dimeric structure **3**. Analytical details are discussed above. Complex **4** is prepared in a two-step synthesis from $Ru_3(CO)_{12}$ with propionic acid and vinyl acetate. The intermediate step is the formation of $[Ru(CO)_2(CH_3CH_2COO)]_n$, which forms the monomeric structure **4** after refluxing with vinyl acetate and propionic acid. The propionate signals appear at a slightly upfield position compared to the isolated carboxylic acid at 1.09 ppm and 2.29 ppm, respectively, in the ^{1}H NMR spectrum (MeOD-d_4). The two binding modes of the propionate ligands result in two superimposed sets of signals. This is even more evident in the ^{13}C NMR spectrum, where the carboxylate C atoms are observed at 178.3 ppm (η^2-CH_3CH_2COO) and 183.4 ppm (η^1-CH_3CH_2COO), respectively, thus exhibiting a difference in the chemical shift of more than 5 ppm. The difference can also be observed at the aliphatic C atoms, but diminishes with increasing distance to the metal center. Due to slow relaxation, only one carbonyl C atom is observed at 198.0 ppm.

Complex **6** was synthesized from $Ru_3(CO)_{12}$ with an excess of pivalic acid in toluene, yielding an orange crystalline product.[19] Single-crystal XRD could be carried out in this work for the first time, confirming the structure of the complex as assigned by Shvo et al. in 1986.[21] Crystallographic data are given in Table 2. Each of the ruthenium atoms is coordinated in a slightly distorted octahedral manner, with two *t*-BuCOOH ligands along the Ru1–Ru2-axis and two bridging *t*-BuCOO ligands connecting both ruthenium atoms. The terminal carboxylic acid protons each form a hydrogen bond to one of the bridging carboxylate ligands, which results in a distortion of the axial pivalic acid ligands towards the bridging carboxylate ligands. This is reflected in the O3–Ru1–Ru1#1 bonding angle of 163.13(4), i.e., well below 180 deg. As indicated in Figure 7, the methyl groups of the bridging pivalate ligands are disordered in the crystal.

^{1}H NMR spectroscopic investigation reveals two separate methyl signals for the *t*-BuCOO and *t*-BuCOOH at 1.13 ppm and 1.25 ppm, which are both shifted slightly upfield compared to the uncoordinated pivalic acid. The acidic protons are observed at 11.46 ppm.

Compound **7** has been synthesized previously by Schumann et al.[22] Single crystal structural analysis is presented here for the first time (Figure 8), crystallographic data are given in Table 2. The complex crystallizes in an orthorhombic structure and exhibits the expected structural features of a dinuclear sawhorse type ruthenium complex. Similar to the dimeric structure **3**, the axial ligands are distorted towards the propionate ligands. This is reflected in the P1–Ru1–Ru2 and P2–Ru2–Ru1 bonding angles below 180 deg.

Table 2. Crystallographic data of complexes **6** and **7**.

	6	**7**
Formula	$C_{12}H_{19}O_6Ru$	$C_{34}H_{64}O_8P_2Ru_2$
Formula wt	360.34	864.93
Space group	*I* 2/*a*	*P bca*
a (Å)	15.2653(3)	18.0933(10)
b (Å)	9.8416(2)	17.7207(9)
c (Å)	21.8388(6)	24.5667(13)
α (deg)	90	90
β (deg)	106.809(1)	90
γ (deg)	90	90
V (Å^3)	3140.77(12)	7876.7(7)
Z	8	8
$D_{calcd.}$ (g cm^{-3})	1.524	1.459
N_{ref}	3877	7206
N_{par}	213	435
R1 ($I > 2\sigma(I)$)	0.0251	0.0202
wR2 (all data)	0.0576	0.0493
Goodness of fit	0.955	1.056

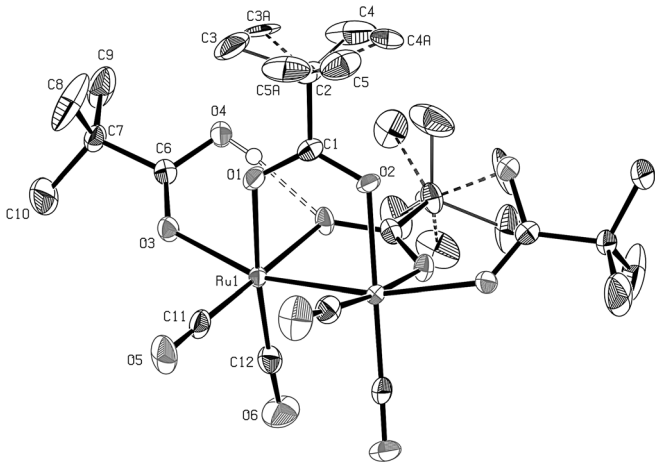

Figure 7. ORTEP representation of $[Ru(CO)_2(t\text{-BuCOO})(t\text{-BuCOOH})]_2$ (**6**).[19] Thermal ellipsoids are shown at the 50% probability level. Protons are omitted for clarity. Selected bond lengths (Å) and bond angles (deg): Ru1–Ru1#1 2.6117(3), Ru1–O3 2.2487(13), Ru1–C11 1.841(2), Ru1–C12 1.832(2), Ru1–O1 2.1280(13), O3–Ru1–Ru1#1 163.13(4), C12–Ru1–C11 88.78(10), C11–Ru1–Ru1#1 97.13(6), O1–Ru1–O3 82.59(5), C12–Ru1–O1 174.23(8), C6–O4–H4 106.1(19).

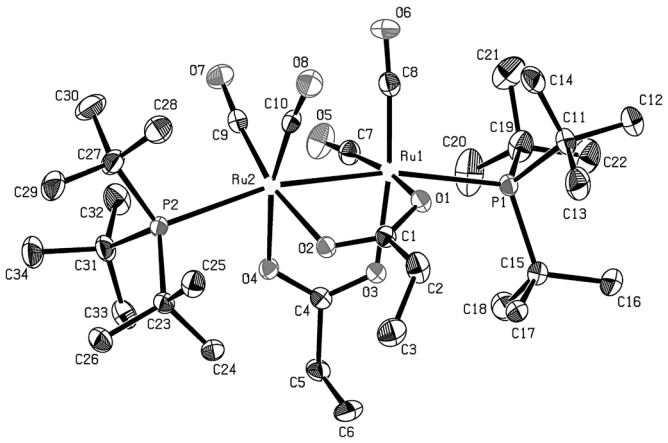

Figure 8. ORTEP representation of $\{Ru(CO)_2(CH_3CH_2COO)[P(t\text{-Bu})_3]\}_2$ (**7**).[22] Thermal ellipsoids are shown at the 50% probability level. Protons are omitted for clarity. Selected bond lengths (Å) and bond angles (deg): Ru1–Ru2 2.7085(2), Ru1–P1 2.5962(5), Ru2–P2 2.5957(5), Ru1–O1 2.1251(13), Ru1–O3 2.1330(13), Ru2–O2 2.1678(13), Ru2–O4 2.1377(13), Ru1–C7 1.842(2), Ru1–C8 1.846(2), Ru2–C9 1.842(2), Ru2–C10 1.832(2), P1–Ru1–Ru2 165.721(13), P2–Ru2–Ru1 165.380(13), O1–Ru1–O3 85.13(5), O4–Ru2–O2 84.50(5), C7–Ru1–O1 170.87(7), C8–Ru1–O3 172.76(7), C10–Ru2–O4 166.86(7), C9–Ru2–O2 168.44(7), C7–Ru1–C8 86.83(9), C10–Ru2–C9 86.85(9).

Within the limits of the experimental error, equivalent bond lengths are equal.

Catalytic Activity

Figure 9 summarizes the results of the kinetic studies. The activity of the sample catalyst species decreases in the order **4** > **5** > **6** > **1** > **3** > **8** > **7**. Interestingly, complex **4**, which corresponds to the mononuclear active species as proposed above, exhibits by far the highest activity, followed by the mononuclear bis(trifluoroacetato) complex **5**. The anionic mononuclear species **1** shows only very little activity, just like all investigated dinuclear complexes. This suggests that uncharged mononuclear species in general may exhibit the highest activities in transvinylation. The reduced activity of **5** compared to **4** may be attributed to the electron-

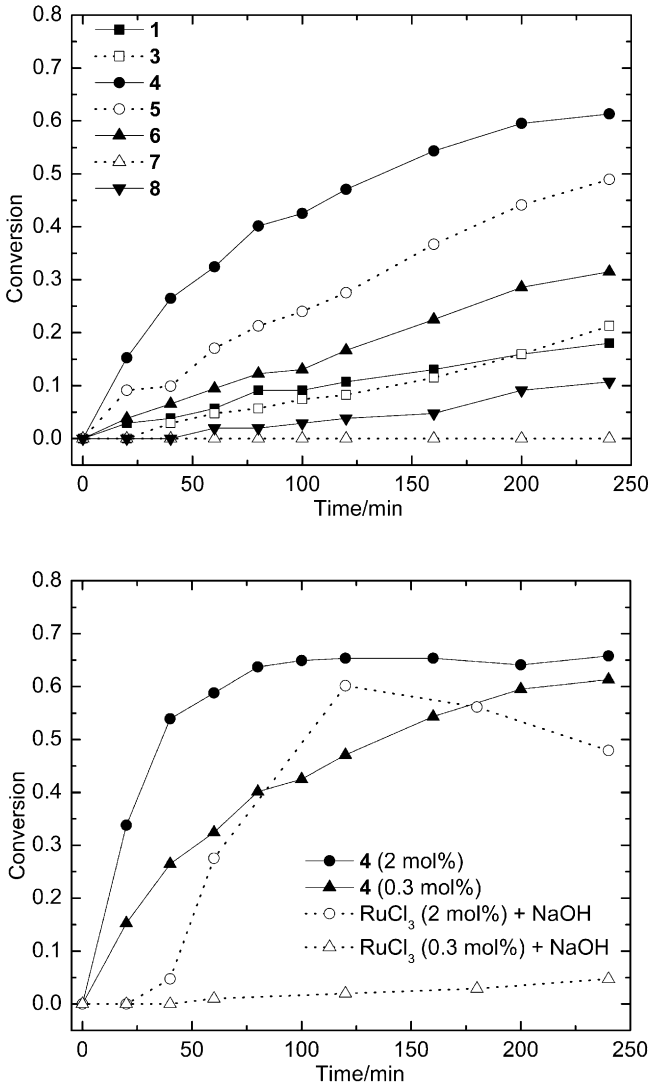

Figure 9. *Top*: Catalytic activity of the model complexes in transvinylation of propionic acid with vinyl acetate. [Ru] = 0.3 mol% referred to propionic acid, propionic acid:vinyl acetate = 1:2.7, $T = 100\,^{\circ}C$. *Bottom:* Comparison of the catalytic activity of **4** and $RuCl_3$ hydrate at [Ru] = 0.3 mol% and 2 mol% in transvinylation of propionic acid with vinyl acetate, propionic acid:vinyl acetate = 1:2.7, $T = 100\,^{\circ}C$.

withdrawing trifluoroacetato ligands. The resulting electron deficiency seems to slow down the activation of the catalyst. This may be attributed to the fact that electron density at the metal center is a crucial parameter for the addition of the vinyl donor to the ruthenium center, as will be discussed below. The dinuclear complexes **3** and **6** and the polymeric species **8** exhibit mediocre activity during catalysis. Considerably slower conversion is observed compared to **4** and **5**. The dinuclear and polynuclear species are assumed to form minor amounts of the mononuclear active species, with the equilibrium shifted clearly towards the dinuclear and polynuclear compounds. The bis(tri-*tert*-butylphosphino) complex **7** is entirely inactive, corresponding to the previously reported very low activity of Ru-phosphino complexes.[13a–c] Alkaline $RuCl_3$ hydrate exhibits a long activation period of roughly 30 min, during which the catalytically active species is formed. After 2 h reaction time, the maximum conversion (62%) for the mixture prepared from $RuCl_3$ hydrate ([Ru] = 2 mol% referred to propionic acid) is observed, after which the transvinylation of the acetic acid formed *in situ* reaches considerable quantities. The fact that ruthenium-catalyzed transvinylation is an equilibrium reaction is evidenced by the drop of vinyl propionate content in solution to 50% after 4 h reaction time.[13d] A comparison of the activity of alkaline $RuCl_3$ hydrate with complex **4** is shown in Figure 9. For induction of significant conversion by alkaline $RuCl_3$ hydrate, a higher molar concentration of Ru is needed compared to the mononuclear species **4**. When [Ru] = 0.3 mol%, only very little conversion is observed for alkaline $RuCl_3$ hydrate, while at [Ru] = 2 mol%, the conversion achieved with both systems is comparable, with the mononuclear species **4** exhibiting the highest activity in transvinylation for all investigated Ru concentrations. Taking into account that the activity of the neutral mononuclear species **5** is second best within the set of catalyst species tested, it may be assumed that mononuclear ruthenium complexes of the type $[Ru(CO)_3(RCOO)_2]$ are responsible for activity in ruthenium-catalyzed transvinylation. Therefore, complex **4** is chosen as model catalyst for the following mechanistic investigations.

Mechanistic Studies

In order to elucidate (i) how the active species is formed from the mixture of $RuCl_3$ hydrate, NaOH, RCOOH, and vinyl acetate, and (ii) how the active species may act in a transvinylation reaction pathway, a series of mechanistic experiments was carried out. These experiments aim to determine the origin of the CO ligands within the active species, the nature of the transferred functional group, regio- and stereoselective aspects as well as relevant electronic and steric influences of the vinyl donor.

Origin of CO Ligands

It has been reported previously that the same active species is formed *in situ* from different Ru precursors.[13c] An important structural feature of the active species appear to be the carbonyl ligands. However, to date it remains unclear how these may be formed from $RuCl_3$ hydrate in transvinylation. By employing ^{13}C-labeling experiments and analysis of the ruthenium products *via* IR and NMR spectroscopy, the origin of the CO ligands was investigated. Four ^{13}C-, respectively, ^{18}O-labeled substrates were used (Scheme 2). The origin of the CO ligands is particularly intriguing because the formation of carbonyl ligands from carboxylate groups of the substrate molecules could be ruled out. However, when vinyl acetate with ^{13}C-labeled vinyl positions was used, ^{13}CO ligands could be detected *via* IR spectroscopy. The isotopic shift of the carbonyl absorption band positions corresponds well to the calculated values within the approximation for a harmonic oscillator (see the Supporting Information, Table S1).

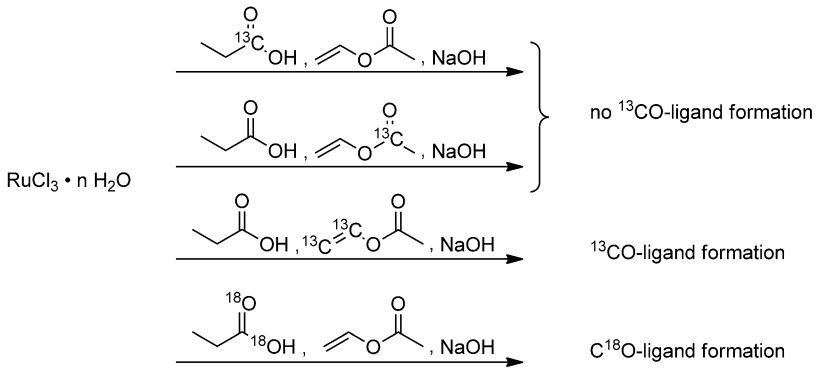

Scheme 2. Investigation of the origin of the CO ligands of the active species.

Table 3. Composition of NMR mixtures to determine the mechanism of the origin of the CO ligands. VAM = vinyl acetate monomer, PA = propionic acid. To every mixture listed, 7.7 mg of $RuCl_3$ hydrate and 0.1 mL of D_2O were added. $V(VAM) + V(propionic\ acid) = 0.4$ mL.

Entry	VAM [equiv.]	PA [equiv.]	NaOH [mg]	CO Signal (^{13}C NMR) [ppm]
1	1.0	–	–	200.0
2	1.0	–	1.5	202.6, 195.1
3	2.7	1.0	1.5	202.7, 194.7
4	–	1.0	–	–
5	–	1.0	1.5	–
6	2.7	1.0	–	202.1, 194.6

This indicates C=C bond activation, cleavage and oxidation at the ruthenium center during the activation period. To elucidate the mechanism and the reactants involved in this unusual CO ligand formation, a series of NMR-scale experiments was carried out (Table 3), mimicking the conditions of the catalytically active reaction mixture but strategically omitting single components. The formation of a carbonyl ligand species from only $RuCl_3$ and vinyl acetate (Entry 1) indicates that the oxygen is not necessarily taken from propionic acid, as might be assumed from the formation of $C^{18}O$ when ^{18}O-labeled propionic acid is used (Scheme 2).

Based on these results, two possible mechanisms for the formation of the active species can be drafted (Scheme 3). Both reaction pathways are initiated by cleavage of the vinyl ester. C–O bond cleavage of vinyl esters at the indicated position has been reported for low-valent ruthenium complexes such as [Ru(cod)(cot)][23] and Ru hydride complexes.[24] Path (a) starts from the assumption that the olefinic carbon atoms may be oxidized to formic acid under the given reaction conditions. The following steps – formation of $[Ru(CO)_2Cl_2]_n$ from $RuCl_3$ hydrate and formic acid[25] as well as the cleavage of the polymeric structure by donor ligands[18c,25b,c] – are well known in the literature. Path (b) proceeds *via* a Wacker-type oxidation of the resulting olefin at a Ru(III) center to form acetaldehyde, which has been reported previously.[26] Formal oxidative addition of acetaldehyde to the ruthenium center and reductive elimination of methane results in the formation of a carbonyl ligand. Decarbonylation of acetaldehyde under release of methane has been reported for Ir(III) systems.[27] At this stage, it remains uncertain along which pathway the reaction proceeds. Further investigations remain necessary to understand in detail how the active catalyst species is formed from $RuCl_3$ hydrate.

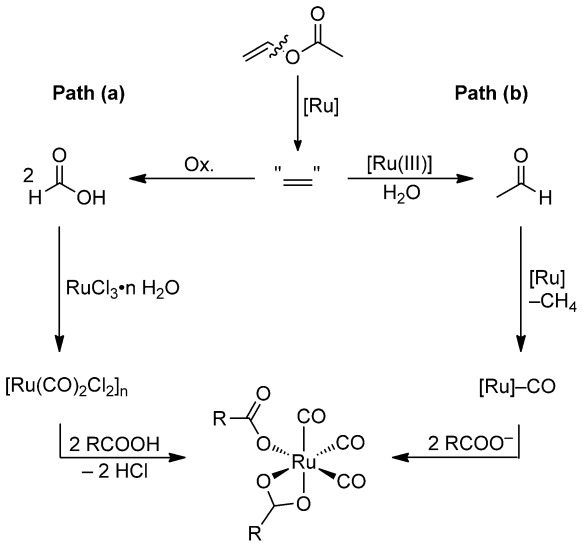

Scheme 3. Possible formation of CO ligands in the active catalyst species.

Investigation of the Transferred Functional Group

Through application of ^{18}O-labeled acetic acid in a model transvinylation experiment (Scheme 4), we found that the vinyl group rather than the vinyloxy group is transferred during transvinylation catalysis. GC-MS measurements provide evidence for the formation of ^{18}O-vinyl acetate, thus demonstrating the transfer of solely a vinyl entity.

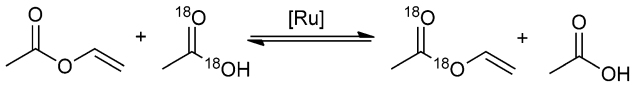

Scheme 4. Reaction scheme for the determination of the transferred functional group using ^{18}O-labeled propionic acid. [Ru] = 0.3 mol% **4**.

Regioselectivity

Regioselectivity during transvinylation is examined using 1-substituted vinyl donors such as isopropenyl acetate as vinyl donor (Scheme 5).

^1H and ^{13}C NMR spectroscopic investigations of the products of the transvinylation cycle reveal isopropenyl propionate to be the main reaction product; ethen-

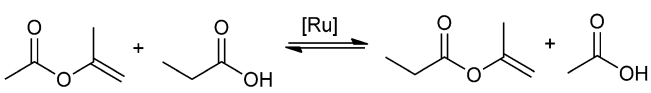

Scheme 5. Reaction scheme for the investigation of the regioselectivity of the reaction. [Ru] = 0.3 mol% **4**.

yl acetate is not observed. Thus, bond cleavage and formation both take place at the same vinyl C atom during transvinylation catalysis at the ruthenium center.

Stereoselectivity

The stereoselectivity of the transvinylation reaction was investigated using a *cis/trans*-mixture (70:30) of butenyl acetate for transvinylation of propionic acid (Scheme 6). During catalysis, both *cis*-butenyl propionate and *trans*-butenyl propionate are formed, indicating a possibility for configuration inversion (see Table 7).

This is in accordance with mechanistic investigations of Pd(II)-catalyzed transvinylation, where a *cis*-insertion of the vinyl donor to the metal complex and subsequent rotation and *cis*-elimination are proposed intermediate steps of the reaction mechanism.[12c] In addition, the percentages of *cis*- and *trans*-butenyl acetate indicate a preferential conversion of *cis*-butenyl acetate over *trans*-butenyl acetate, with a clear possibility for configuration inversion in the product mixture. These results can best be summed up in a mechanism (Scheme 7) similar to the results published by Sabel et al. concerning Pd(II)-catalyzed transvinylation.[12c]

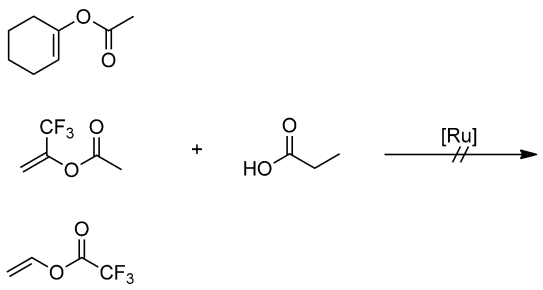

Scheme 8. Inactive vinyl ester compounds with sterically demanding and electron-withdrawing groups. [Ru] = 0.3 mol% **4**.

Variation of the Vinyl Donor

Variation of the substituents of the vinyl donor was used to narrow down the electronic and steric requirements for transvinylation at the ruthenium center. None of the electronically or sterically deactivated vinyl esters displayed in Scheme 8 reacted under transvinylation conditions. This indicates (i) that sufficient electron density at the vinyl group is necessary for successful transvinylation and (ii) that sterically demanding residues can prevent the interaction of the metal center and the vinyl group entirely. It is interesting to note that vinyl trifluoroacetate cannot be converted even though complex **5** is an effective catalyst. This may be attributed to the low electron density at the vinyl double bond, which is crucial for the transvinylation reaction to proceed

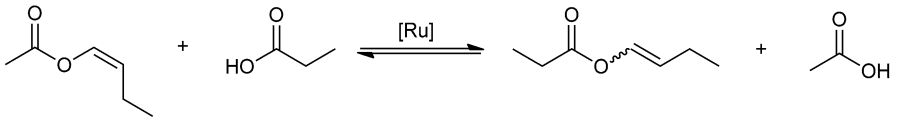

Scheme 6. Reaction scheme for the investigation of the stereoselectivity of the reaction. [Ru] = 0.3 mol% **4**.

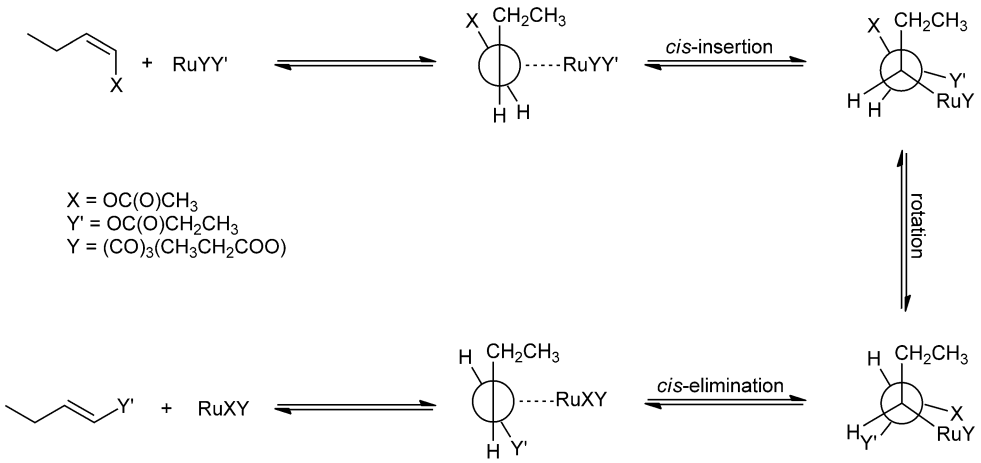

Scheme 7. Proposed reaction mechanism taking into account the stereoselectivity of the reaction.

(see below). The high activity of **5**, on the other hand, is due to its beneficial structural features, which predominate the electron-withdrawing effect of the trifluoroacetate ligands.

DFT Calculations

To elucidate the reaction mechanism, a DFT study was carried out. According to previous observations made and the catalytic activities of known complexes with different structural motifs (see above), a neutral monomeric tris(carbonyl) species has been presumed as active species. Generally, two coordination modes of vinyl acetate to the catalyst are possible: either *via* the vinyl group or the carboxylic oxygen atom to which the vinyl group is bound. Coordination *via* the remaining carboxylate oxygen atom was ruled out as a result of the experimental evidence for transfer of the vinyl group only as opposed to the vinyloxy group (see above). Furthermore, it was attempted to find a mechanism including oxidative addition of vinyl acetate to the Ru center followed by reductive elimination of vinyl propionate. However, several attempts with a separated third carboxyl group failed to converge. Instead, a 7-coordinated Ru intermediate bearing three carboxylic groups and possible transition states was found. As the free energy of this intermediate is already above 320 kJ mol^{-1} with respect to the starting material, and the transition states are found above 350 kJ mol^{-1}, this pathway was excluded from further investigations. This is consistent with the results for cycle 1 (Scheme 9, *left*) where the highest transition state of the outer sphere vinyl exchange mechanism exhibits a relative free energy of 270 kJ mol^{-1} (see below).

Both possible reaction mechanisms, which can be drafted from these observations, are presented in Scheme 9. They were investigated *via* DFT calculations using the B3LYP/6-31G* level of theory.

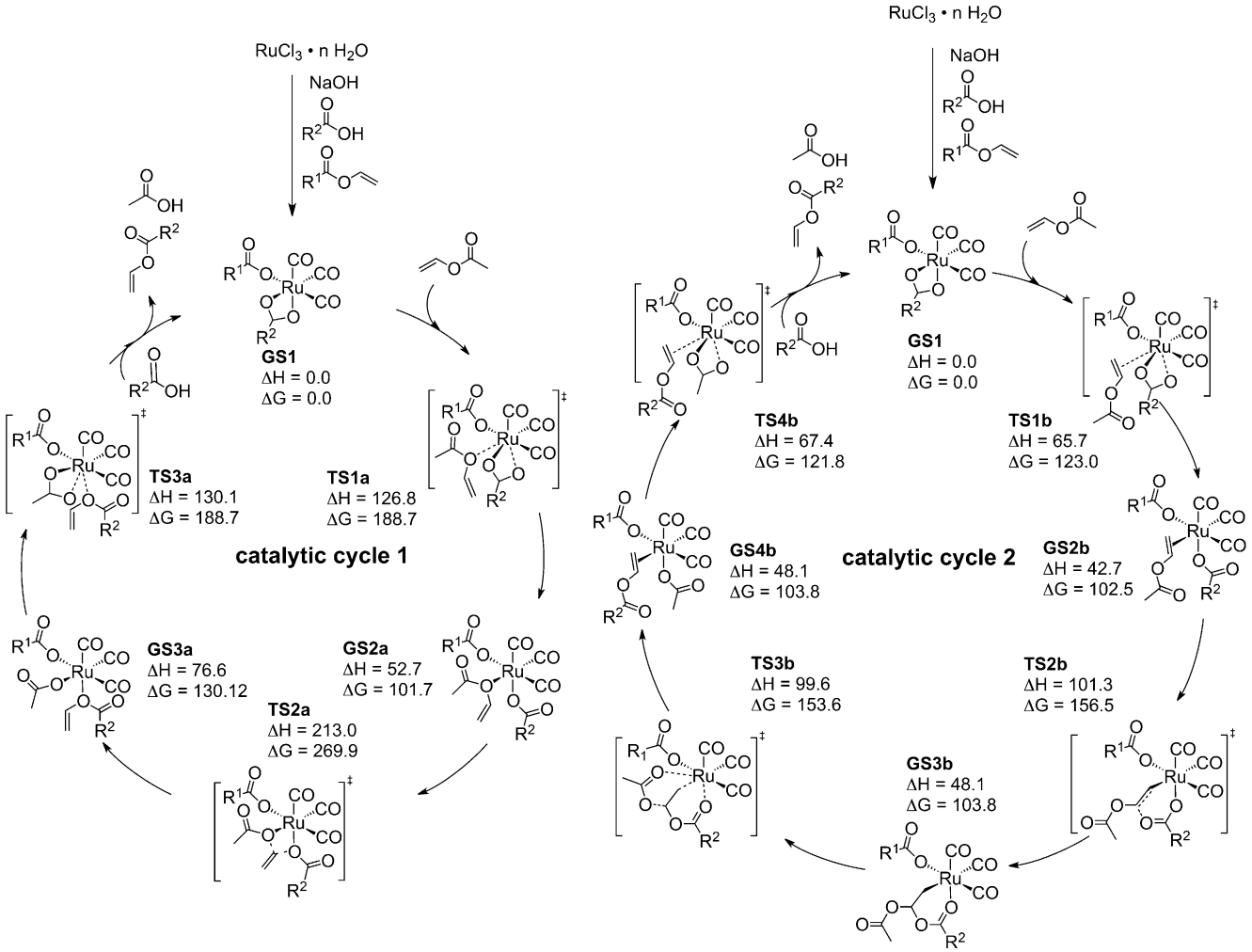

Scheme 9. Possible transvinylation reaction mechanisms incorporating coordination of the vinyl donor *via* carboxylate oxygen (*left*, catalytic cycle 1) and *via* the vinyl group (*right*, catalytic cycle 2). All energy values are given in kJ mol^{-1}.

In cycle 1, the vinyl donor coordinates with the oxygen atom adjacent to the vinyl group (**TS1a**) and the vinyl transfer takes place directly from one carboxylate to the other. This reaction pathway entails a four-membered transition state (**TS2a**) where vinyl transfer is carried out. On the other hand, the key transition and intermediate states in cycle 2 (**TS2b**, **GS3b**, **TS3b**) comprise a six-membered ring, which is formed *via* addition of the Ru center and one of its carboxylate ligands to the vinyl double bond. Experimental evidence indicates that bond cleavage and formation both take place at the same C atom. Therefore, the carboxylate ligand must bind to the vinyl C atom adjacent to the carboxylate group (see above). The respective vinyl carboxylate is formed and cleaved from the Ru center. The graphs displayed in Figure 10 represent the relative free energies and relative enthalpies of the subsequent ground and transition states. Looking at the ΔG scale, the addition of the vinyl ester in the first step is the rate-determining step in both cycles, representing the highest single barrier compared to the corresponding other transition states of the respective cycle. On the ΔH scale, this is true only for cycle 2, while in cycle 1 the vinyl transfer *via* the four-membered cyclic transition state (**TS2a**) requires the highest activation enthalpy. Considering the rate-determining steps, the preference of cycle 2 is evident already at this stage. The activation enthalpies in cycle 2 are between 19 kJ mol^{-1} and 66 kJ mol^{-1} and are thus much lower than in cycle 1 (54 kJ mol^{-1} to 160 kJ mol^{-1}). It is evident from the computed energies that coordination *via* the vinyl group in the first step of the reaction pathway is energetically much more favorable than coordination *via* the carboxylate oxygen atom. Moreover, the vinyl transfer runs *via* the low-energy pathway when the original coordination takes place at the vinyl group. This may be attributed to the much lower ring tension in the six-membered ring transition states **TS2b** and **TS3b** in cycle 2 compared to the four-membered transition state **TS2a** in cycle 1. Based on these results, we propose catalytic cycle 2 as the most likely reaction mechanism for ruthenium-catalyzed transvinylation.

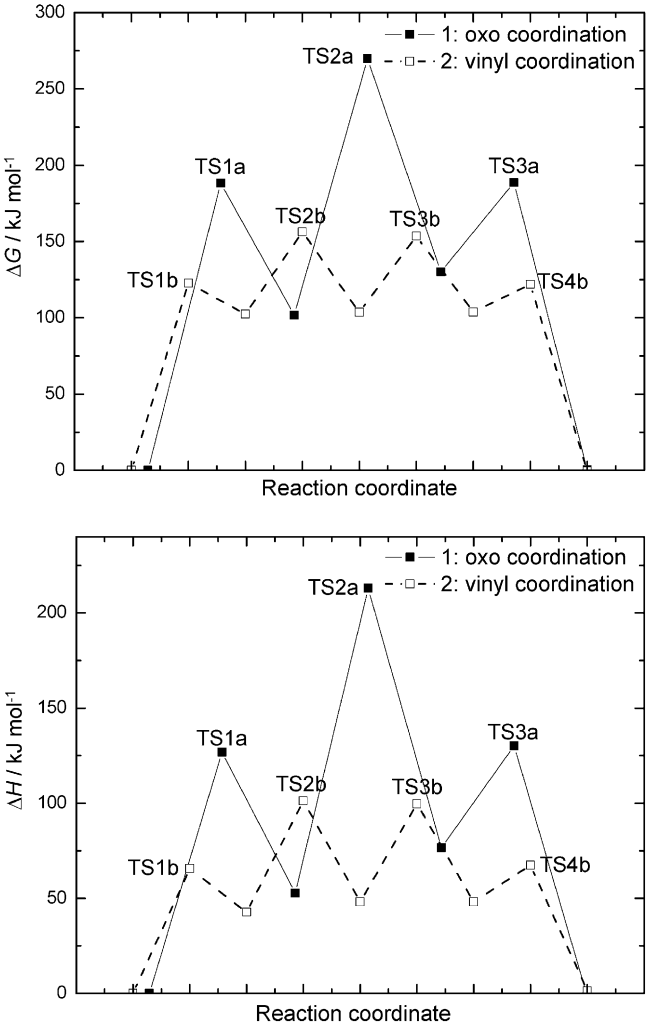

Figure 10. Free energies (*top*) and enthalpies (*bottom*) of ground and transition states in catalytic cycle 1 (black squares, oxo coordination) and catalytic cycle 2 (open squares, vinyl coordination).

Conclusions

With this study new insights into the mechanism of ruthenium-catalyzed transvinylation are provided. Three new ruthenium complexes including two crystal structures as well as crystal structures of two previously known ruthenium complexes are presented. The most likely catalytically active species is identified and characterized. A reaction mechanism is proposed based on analysis of ruthenium species formed from $RuCl_3$ hydrate, the results of a series of isotope labeling experiments, regio- and stereoselective investigations and DFT calculations (Scheme 10). Based on these results, it might be possible to develop catalysts with a more rational design approach than the ruthenium precursors, which are currently in use. Since the exchange of the carboxylate ligand is crucial for transvinylation catalysis, immobilization might be possible through adequate replacement of the carbonyl ligands.

Experimental Section

General Remarks

Commercially available solvents and reagents were used as delivered. Unless otherwise noted, all reactions were carried out under an argon atmosphere. $RuCl_3$ hydrate was obtained from Sigma–Aldrich and used without further purification.

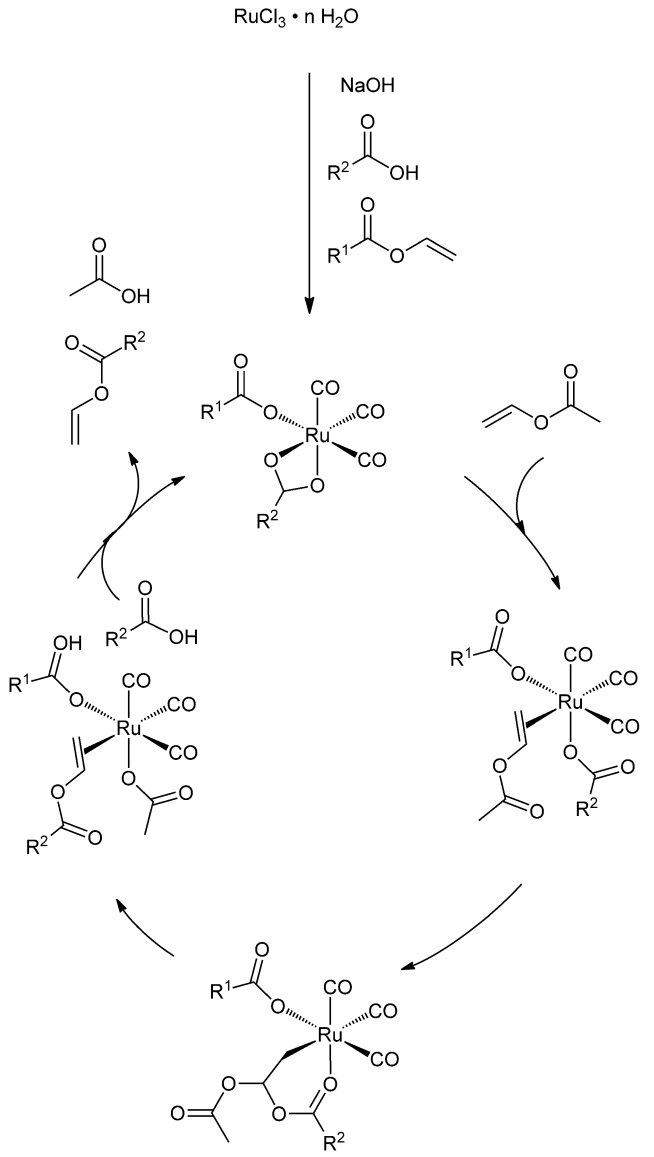

Scheme 10. Proposed mechanism for ruthenium-catalyzed transvinylation.

$Ru_3(CO)_{12}$ was obtained from ABCR and used without further purification. Elemental analyses were obtained from the Microanalytical Laboratory of Technische Universität München. Spectroscopic data were recorded on the following instruments: IR spectra: Jasco FT/IR 460 PLUS; NMR spectra: Bruker DPX-400 and Bruker Avance III 400 (^{1}H NMR 400.13 MHz, ^{13}C NMR 100.53 MHz, ^{31}P NMR 100.61 MHz), $T = 300$ K. Signals were calibrated to the residual proton resonance or the natural abundance ^{13}C resonance of the solvent, respectively.[26] Signal multiplicities are abbreviated as: s (singlet), d (doublet), t (triplet), q (quartet), quint (quintet), m (multiplet), br (broad). ESI-mass spectra were recorded on a ThermoElectron LCQ classic. GC-mass spectra were recorded on a Hewlett–Packard chromatograph HP6890 using chloroform as a solvent. CCDC 940441, CCDC 940442,CCDC 940443 and CCDC 940444 contain the supplementary crystallographic data for this paper. These data can be obtained free of charge from The Cambridge Crystallographic Data Centre *via* www.ccdc.cam.ac.uk/data_request/cif. Crystallographic details are given in the supporting information.

Preparation of the Catalytically Active Crude Mixture

100 mg $RuCl_3 \cdot n\,H_2O$ (0.48 mmol, 1.0 equiv.) and 20 mg NaOH (0.50 mmol, 1.3 equiv.) were suspended in 5 mL vinyl acetate (54 mmol) and 1.5 mL propionic acid (20 mmol) or 2.2 mL valeric acid (20 mmol), respectively, were added to the mixture. The solution was heated to 140 °C in a pressure tube for 4 h and then slowly cooled to room temperature. The reaction was performed on air. For further analysis, the brown suspension was dried under vacuum. For analytical details and spectra, see the Supporting Information.

Isolation of Na[*fac*-Ru(CO)$_3$(RCOO)$_3$] (R = CH$_3$, CH$_2$CH$_3$ 1:1) (1)

100 mg $RuCl_3 \cdot n\,H_2O$ (0.48 mmol, 1.0 equiv.) and 20 mg NaOH (0.50 mmol, 1.0 equiv.) were suspended in 5 mL vinyl acetate (54 mmol) and 1.5 mL of propionic acid (20 mmol) were added to the mixture. The solution was heated to 140 °C in a pressure tube for 4 h and then slowly cooled to room temperature. The mixture was filtered and concentrated under vacuum to give a dark red-brown oil, to which 3 mL of diethyl ether were added. After vigorous stirring, the resulting solid was washed with pentane (5 × 3 mL) and recrystallized from THF; yield: 102 mg (0.23 mmol, 53%); $C_{12}H_{15}NaO_9Ru$ (427.30)/$C_9H_9NaO_9Ru$ (385.22) crystal: anal. calcd.: C 32.33%, H 3.29%; found: C 32.37%, H 3.36%; IR (KBr): $\nu = 2127$ (s), 2049 (vs), 1614 (s), 1375 (m), 1329 (m), 686 (w), 624 (w), 580 cm^{-1} (w); ^{1}H NMR (400 MHz, MeOD): $\delta = 1.10$ (t, $^3J_{H,H} = 7.6$ Hz, 3H, CH_2CH_3), 1.99 (s, 3H, CH_3COO), 2.30 (q, $^3J_{H,H} = 7.5$ Hz, 2H, CH_2CH_3); ^{13}C NMR (101 MHz, MeOD): $\delta = 196.2$ (*C*O), 178.4 (CH_3CH_2COO), 175.3 (CH_3COO), 28.2 (CH_3CH_2COO), 20.8 (CH_3COO), 9.5 (CH_3CH_2COO).

Isolation of [Ru(CO)$_2$(μ-η^2-CH$_3$CH$_2$COO)]$_n$

Water was added to the filtered and concentrated catalytically active crude mixture (see above) until an orange solid precipitated out. This solid was washed with diethyl ether and dried under vacuum; yield: 4%. Satisfactory analytical data were obtained.[17]

[Ru(CO)$_2$(μ-η^2-CH$_3$(CH$_2$)$_3$COO)]$_n$ (2)

Water was added to the catalytically active crude mixture (see above) until an orange solid precipitated out. This solid was washed with diethyl ether and dried under vacuum. For synthetic purposes, 100 mg $Ru_3(CO)_{12}$ (0.16 mmol, 1.0 equiv.) were suspended in 6 mL valeric acid (5.6 g, 55 mmol) and the mixture was heated under reflux conditions for 12 h. After removal of all volatiles and washing with diethyl ether (4 × 5 mL), the product was obtained as an orange solid; yield: (113 mg (0.22 mmol, 92%); $(C_{14}H_{18}O_8Ru_2)_n$ (516.43); anal. calcd.: C 32.56%, H 3.51%; found: C 32.74%, H 3.50%: IR (KBr): $\nu = 2039$ (s), 1993 (s), 1969 (s), 1941 (m), 1546 (s), 1412 cm^{-1} (m); ^{1}H NMR

(400 MHz, CD_3COOD): $\delta = 0.95$ (t, $^3J_{H,H} = 7.6$ Hz, 3H, CH_3CH_2), 1.39 (m, 2H, CH_3CH_2), 1.63 (m, 2H, CH_2CH_2COO), 2.39 (t, $^3J_{H,H} = 7.2$ Hz, 2H, CH_2COO); ^{13}C NMR (101 MHz, THF-d_8): $\delta = 202.7$ (*C*O), 186.4 (*C*OO), 36.9 (*C*H_2COO), 29.1 (*C*H_2CH_2COO), 23.1 (CH_3CH_2), 14.1 (*C*H_3).

$[Ru(CO)_2(\mu\text{-}\eta^2\text{-}CH_3CH_2COO)(dmso)]_2$ (3)

30 mg $[Ru(CO)_2(CH_3CH_2COO)]_n$ (0.13 mmol, 1.0 equiv.) were dissolved in 0.2 mL DMSO at 80 °C. After cooling to 4 °C overnight, the yellow crystals were filtered off and washed with pentane; yield: 14 mg (0.02 mmol, 18%); $C_{14}H_{22}O_{10}Ru_2S_2$ (616.87); anal. calcd.: C 27.27%, H 3.60%, S 10.37%; found: C 27.56%, H 3.69%, S 10.65%; IR (KBr): $\nu = 2037$ (s), 1997 (m), 1971 (s), 1943 (m), 1558 (s), 1433 (m), 1243 (s), 1102 (s), 1022 cm^{-1} (s); ^1H NMR (400 MHz, $CDCl_3$): $\delta = 1.03$ (t, $^3J_{H,H} = 7.5$ Hz, 3H, CH_2CH_3), 2.29 (q, $^3J_{H,H} = 7.4$ Hz, 2H, CH_2CH_3), 3.00 (s, 6H, SCH_3); ^{13}C NMR (101 MHz, $CDCl_3$): $\delta = 200.6$ (*C*O), 189.0 (*C*$OOCH_2CH_3$), 42.4 ($OS(CH_3)_2$), 30.7 (CH_2CH_3), 10.9 (CH_2CH_3).

[*fac*-$Ru(CO)_3(\eta^2\text{-}CH_3CH_2COO)(\eta^1\text{-}CH_3CH_2COO)$] (4)

100 mg $Ru_3(CO)_{12}$ (0.16 mmol, 0.33 equiv.) were suspended in 5 mL propionic acid and heated for 12 h to 100 °C. After evaporating all volatiles under vacuum, 2 mL of propionic acid and 6 mL of vinyl acetate were added to the yellow solid and the mixture was heated to 70 °C for 2 h. Volatiles were evaporated under vacuum and the resulting colorless solid washed with pentane (5 × 2 mL); yield: 97 mg (0.29 mmol, 62%); $C_9H_{10}O_7Ru$ (331.95)·0.5 H_2O; anal. calcd. C 31.77%, H 3.26%; found: C 31.62%, H 3.35%; IR: $\nu =$ 2132 (w), 2055 (s), 1984 (s), 1520 (s), 1413 cm^{-1} (s); ^1H NMR (400 MHz, MeOD): $\delta = 1.08$ (m, 3H, CH_2CH_3), 2.29 (q, $^3J_{H,H} = 7.6$ Hz, 2H, CH_2CH_3); ^{13}C NMR (101 MHz, MeOD): $\delta = 198.0$ (*C*O), 183.4 (η^1-CH_3CH_2COO), 178.3 (η^2-CH_3CH_2COO), 30.0 (η^1-CH_3CH_2COO), 28.1 (η^2-CH_3CH_2COO), 11.1 (η^1-CH_3CH_2COO), 9.5 (η^2-CH_3CH_2COO).

Catalyses

See Table 4, Table 5, Table 6, and Table 7.

Table 4. Catalytic transvinylation of propionic acid with isopropenyl acetate (1:3) with 0.3 mol% **4** as catalyst. Conversion was determined using ^1H NMR spectroscopy in acetone-d_6. Propionic anhydride was observed as side-product.

Time [min]	Conversion
0	0
15	1
30	7
45	12
70	18
130	37
190	47

Table 5. Overview over catalyzed transvinylation of propionic acid with vinyl acetate. Conversion was determined using ^1H NMR spectroscopy in acetone-d_6.

Cat.: Time [min]	**1**	**3**	**4**	**5**	**6**	**7**	**8**
0	0	0	0	0	0	0	0
20	2.9	0	15.3	9.1	3.8	0	0
40	3.8	2.9	26.5	9.9	6.5	0	0
60	5.7	4.8	32.4	17.1	9.5	0	2.0
80	9.1	5.7	40.1	21.3	12.3	0	2.0
100	9.1	7.4	42.5	24.0	13.0	0	2.9
120	10.7	8.3	47.1	27.5	16.7	0	3.8
160	13.0	11.5	54.3	36.7	22.5	0	4.8
200	16.0	16.0	59.5	44.1	28.6	0	9.1
240	18.0	21.3	61.4	49.0	31.5	0	10.7

Table 6. Overview over catalyzed transvinylation of propionic acid with vinyl acetate using alkaline $RuCl_3$ hydrate (**9**) and **4**. Conversion was determined using ^1H NMR spectroscopy in acetone-d_6.

Cat.: Time [min]	**9**[a]	**9**[b]	**4**[a]	**4**[b]
0	0	0	0	0
20	0	0	15.3	33.8
40	0	4.7	26.5	53.9
60	1.0	27.5	32.4	58.8
80			40.1	63.7
100			42.5	64.9
120	2.0	60.2	47.1	65.4
160			54.3	65.4
180	3.0	56.1		
200			59.5	64.1
240	4.7	47.9	61.4	65.8

[a] [Ru] = 0.3 mol%.
[b] [Ru] = 2 mol% referred to propionic acid.

Table 7. Overview over catalyzed transvinylation of propionic acid with *cis/trans*-butenyl acetate (70:30) with 0.3 mol% [*fac*-$Ru(CO)_3(\eta^2\text{-}CH_3CH_2COO)(\eta^1\text{-}CH_3CH_2COO)$] (**4**) as catalyst. Conversion was determined using ^1H NMR spectroscopy in $CDCl_3$.

Time [min]	*trans*-butenyl acetate [%]	*cis*-butenyl acetate [%]	*trans*-butenyl propionate [%]	*cis*-butenyl propionate [%]
0	29.5	70.5	0	0
30	30.0	70.0	0	0
60	31.0	69.0	0	0
120	32.9	67.1	0	0
240	31.9	60.2	3.0	4.8
360	32.6	57.1	4.0	6.3
570	35.2	47.6	7.1	10.0
1230	38.4	30.9	16.0	15.2

Computational Details

All calculations have been performed with *Gaussian03*.[28] The level of theory contains the hybrid DFT functional B3LYP[29] and the double zeta 6–31G*[30] basis set for all atoms except Ru. The Stuttgart97-ECP[31] has been applied for the Ru metal centers. All optimized stationary points have been checked by frequency calculations if they represent a transition state (NImag = 1) or a ground state (NImag = 0). Enthalpies and Gibbs free energies are given in kJ mol^{-1} with respect to all starting material of a given catalytic cycle. They have been calculated in gas phase for $T = 298.15$ K and 1 atm. The simulated IR spectra have been taken unscaled from the calculated frequencies of the model compounds.

Acknowledgements

The authors, particularly J. Z. and T. K. Z. are grateful for the financial support of this project provided by the Wacker Chemie AG and appreciate the support of F. Marr and P. Gigler. J. Z., S. H. and D. J. thank the TUM Graduate School and NanoCat – an international doctorate college of the Elite Network Bavaria (ENB). M. D. acknowledges the provision of computing time by the Leibniz Computing Centre (LRZ) of the Bavarian Academy of Sciences.

References

[1] R. E. Neff, R. G. Ryles, European Patent EP 0311799 A1, **1988**.
[2] I. M. Nunez, J. G. Linhardt, J. A. McGee, J. Hunt, M. Alton, D. A. Shipp, J. F. Kunzler, D. M. Ammon, *Patent* WO 2010/147864 A2, **2010**.
[3] J. Ahlgren, N. Bruun, V. Buutinen, *Patent* WO 2010/058087 A1, **2010**.
[4] C.-B. Ko, Y.-M. Kim, K.-J. Song, K.-H. Lee, U.S. Patent 2010/0048077 A1, **2010**.
[5] a) W. J. Kerr, M. McLaughlin, P. L. Pauson, S. M. Robertson, *J. Organomet. Chem.* **2001**, *630*, 104–117; b) H. Yang, E. Henke, U. T. Bornscheuer, *J. Org. Chem.* **1999**, *64*, 1709–1712; c) J. J. Snuparek, J. Mleziva, *Angew. Makromol. Chem.* **1970**, *12*, 145–156.
[6] a) W. Kitching, Z. Rapport, S. Winstein, W. G. Young, *J. Am. Chem. Soc.* **1966**, *88*, 2054–2055; b) I. Nicolau, P. M. Colling, L. R. Johnson, Patent WO 94/08714, **1994**; c) X. Lu, G. Zhu, S. Ma, *Tetrahedron Lett.* **1992**, *33*, 7205–7206.
[7] P. F. Hudrlik, A. M. Hudrlik, *J. Org. Chem.* **1973**, *38*, 4254–4258.
[8] M. Rotem, Y. Shvo, *Organometallics* **1983**, *2*, 1689–1691.
[9] C. Bianchini, A. Meli, M. Peruzzini, F. Zanobini, *Organometallics* **1990**, *9*, 1155–1160.
[10] H. Nakagawa, Y. Okimoto, S. Sakaguchi, Y. Ishii, *Tetrahedron Lett.* **2003**, *44*, 103–106.
[11] R. Adelman, *J. Org. Chem.* **1949**, *14*, 1057–1077.
[12] a) J. E. McKeon, P. Fitton, A. A. Griswold, *Tetrahedron* **1972**, *28*, 227–232; b) J. E. McKeon, P. Fitton, *Tetrahedron* **1971**, 233–238; c) A. Sabel, J. Smidt, R. Jira, H. Prigge, *Chem. Ber.* **1969**, *102*, 2939–2950; d) J. Smidt, W. Hafner, R. Jira, R. Sieber, J. Sedlmeier, A. Sabel, *Angew. Chem.* **1962**, *74*, 93–128.
[13] a) R. E. Murray, U.S. Patent 005155253 A, **1991**; b) R. E. Murray, European Patent EP O0506070 A2, **1992**; c) R. E. Murray, European Patent EPO0351603 A2, **1989**; d) R. E. Murray, D. M. Lincoln, *Catal. Today* **1992**, *13*, 93–102.
[14] T. Funaioli, C. Cavazza, F. Marchetti, G. Fachinetti, *Inorg. Chem.* **1999**, *38*, 3361–3368.
[15] G. B. Deacon, R. J. Phillips, *Coord. Chem. Rev.* **1980**, *33*, 227–250.
[16] A. John, G. Wilkinson, *Polyhedron* **1989**, *8*, 597–602.
[17] G. R. Crooks, B. F. G. Johnson, J. Lewis, I. G. Williams, G. Gamlen, *J. Chem. Soc. A* **1969**, 2761–2766.
[18] a) R. W. Hilts, S. J. Sherlock, M. Cowie, E. Singleton, M. M. de V. Steyn, *Inorg. Chem.* **1990**, *29*, 3161–3167; b) S. J. Sherlock, M. Cowie, *Organometallics* **1988**, *7*, 1663–1666; c) B. Therrien, G. Süss-Fink, *Coord. Chem. Rev.* **2009**, *253*, 2639–2664.
[19] M. Rotem, Y. Shvo, I. Goldberg, U. Shmueli, *Organometallics* **1984**, *3*, 1758–1759.
[20] R. Brückner, *Organic Mechanisms*, Springer, Heidelberg, **2010**.
[21] M. Rotem, I. Goldberg, U. Shmueli, Y. Shvo, *J. Organomet. Chem.* **1986**, *314*, 185–212.
[22] H. Schumann, J. Opitz, J. Pickardt, *J. Organomet. Chem.* **1977**, *128*, 253–264.
[23] J. G. Planas, T. Marumo, Y. Ichikawa, M. Hirano, S. Komiya, *J. Chem. Soc. Dalton Trans.* **2000**, 2613–2625.
[24] S. Komiya, A. Yamamoto, *J. Organomet. Chem.* **1975**, *87*, 333–339.
[25] a) G. N. Krishnamurthy, N. Shashikala, *J. Serb. Chem. Soc.* **2009**, *74*, 1085–1096; b) D. Mulhern, Y. Lan, S. Brooker, J. F. Gallagher, H. Görls, S. Rau, J. G. Vos, *Inorg. Chim. Acta* **2006**, *359*, 736–744; c) C. M. Kepert, G. B. Deacon, L. Spiccia, G. D. Fallon, B. W. Skelton, A. H. White, *J. Chem. Soc. Dalton Trans.* **2000**, 2867–2873; d) P. A. Anderson, G. B. Deacon, K. H. Haarmann, F. R. Keene, T. J. Meyer, D. A. Reitsma, B. W. Skelton, G. F. Strouse, N. C. Thomas, J. A. Treadway, A. H. White, *Inorg. Chem.* **1995**, *34*, 6145–6157.
[26] M. M. T. Kahn, A. P. Rao, *J. Mol. Catal.* **1988**, *44*, 95–105.
[27] a) A. E. Roa, V. Salazar, J. López-Serrano, E. Oñate, M. Paneque, M. L. Poveda, *Organometallics* **2012**, *31*, 716–721; b) P. J. Alaimo, B. A. Arndtsen, R. G. Bergman, *Organometallics* **2000**, *19*, 2130–2143; c) M. A. Garralda, *Dalton Trans.* **2009**, 3635–3645.
[28] M. J. Frisch, G. W. Trucks, H. B. Schlegel, G. E. Scuseria, M. A. Robb, J. R. Cheeseman, J. A. Montgomery Jr, T. Vreven, K. N. Kudin, J. C. Burant, J. M. Millam, S. S. Iyengar, J. Tomasi, V. Barone, B. Mennucci, M. Cossi, G. Scalmani, N. Rega, G. A. Petersson, H. Nakatsuji, M. Hada, M. Ehara, K. Toyota, R. Fukuda, J. Hasegawa, M. Ishida, T. Nakajima, Y. Honda, O. Kitao, H. Nakai, M. Klene, X. Li, J. E. Knox, H. P. Hratchian, J. B. Cross, V. Bakken, C. Adamo, J. Jaramillo, R. Gomperts, R. E. Stratmann, O. Yazyev, A. J. Austin, R. Cammi, C. Pomelli, J. W. Ochterski, P. Y. Ayala, K. Morokuma, G. A. Voth, P. Salvador, J. J.

Dannenberg, V. G. Zakrzewski, S. Dapprich, A. D. Daniels, M. C. Strain, O. Farkas, D. K. Malick, A. D. Rabuck, K. Raghavachari, J. B. Foresman, J. V. Ortiz, Q. Cui, A. G. Baboul, S. Clifford, J. Cioslowski, B. B. Stefanov, G. Liu, A. Liashenko, P. Piskorz, I. Komaromi, R. L. Martin, D. J. Fox, T. Keith, M. A. Al-Laham, C. Y. Peng, A. Nanayakkara, M. Challacombe, P. M. W. Gill, B. Johnson, W. Chen, M. W. Wong, C. Gonzalez, J. A. Pople, *Gaussian03*, Gaussian, Inc., Wallingford, CT, **2004**.

[29] a) A. D. Becke, *J. Chem. Phys.* **1993**, *98*, 5648–5652; b) C. Lee, Y. W, R. G. Parr, *Phys. Rev. B: Condens. Matter* **1988**, *37*, 785–789.

[30] J. Hehre, R. Ditchfield, J. A. Pople, *J. Chem. Phys.* **1972**, *56*, 2257–2261.

[31] M. Dolg, H. Stoll, H. Preuss, R. M. Pitzer, *J. Phys. Chem.* **1993**, *97*, 5852–5859.

